Catalysis Today 171 (2011) 251–256

Contents lists available at ScienceDirect

Catalysis Today

journal homepage: www.elsevier.com/locate/cattod

Role of the ceria promoter and carrier on the functionality of Cu-based catalysts in the CO_2-to-methanol hydrogenation reaction

Giuseppe Bonura[a], Francesco Arena[a,b,*], Giovanni Mezzatesta[b], Catia Cannilla[a], Lorenzo Spadaro[a,b], Francesco Frusteri[a]

[a] CNR-ITAE, Istituto di Tecnologie Avanzate per l'Energia "Nicola Giordano", Salita S. Lucia sopra Contesse 5, 98126 Messina, Italy
[b] Dipartimento di Chimica Industriale ed Ingegneria dei Materiali, Università degli Studi di Messina, Viale F. Stagno D'Alcontres 31, 98166 Messina, Italy

ARTICLE INFO

Article history:
Received 25 October 2010
Received in revised form 19 April 2011
Accepted 27 April 2011
Available online 1 June 2011

Keywords:
CO_2 hydrogenation
Methanol
Cu-catalysts
Oxide promoters
Carrier composition
Oxide/metal interface
Active sites
Reaction mechanism

ABSTRACT

The effects of ZnO or CeO_2 promoters and carrier composition ($Zr_xCe_{(1-x)}O_2$, $0 \le x \le 1$) on the structure and CO_2-hydrogenation functionality (T_R, 453–513 K; P_R, 3.0 MPa; GHSV, 8.8 N L g^{-1} h^{-1}) of Cu/ZrO_2 and Cu–ZnO catalysts respectively have been addressed. The influence of the reduction atmosphere (5 or 100% H_2) on metal surface area (MSA) and activity pattern has been probed. ZnO acts as promoter of both structural and catalytic properties of the metal Cu phase, while the replacement of zirconia carrier with ceria depresses both surface area (SA) and MSA of the Cu–ZnO system. Higher surface methanol yields point out a remarkable promoting effect of ceria on the activity of the Cu–ZnO system, while unsystematic effects of the activation atmosphere on MSA and functionality of the various systems rely on the *dual-site* nature of the main reaction path involving metal and oxide sites at metal/oxide interface.

1. Introduction

The need to cut down the *greenhouse-gas* emissions is pressing a great global scientific concern on novel catalytic technologies allowing an effective conversion and recycle of carbon dioxide [1]. In particular, the CO_2 conversion to methanol looks particularly attractive due to its extensive use for synthesizing liquid fuels (hydrocarbons, dimethylether, etc.) alternative to oil-derived ones and several bulk chemicals (formaldehyde, MTBE, acetic acid, etc.) requiring a current production of ca. 40 Mt/y [1]. Nevertheless, the potential use of methanol and derivatives (DME) as fuels for the automotive sector leads to forecast an impressive growth in methanol demand up to 1500 Mt/y [2]. Then, the synthesis of methanol from CO_2-rich syngas streams, produced either by the catalytic partial oxidation instead of the energy-intensive steam reforming or by reforming/gasification of alternative feedstocks such as coal and biomass, would represent a decisive technological breakthrough with a remarkable improvement of the overall processes economics [3–5]. In fact, methanol is currently produced at industrial scale by feeding syngas streams (CO/H_2) containing minor amounts (<5%) of CO_2 on Cu–ZnO/Al_2O_3 catalysts operating at 493–573 K and 5–10 MPa [6–10]. However their unsatisfactory CO_2-hydrogenation performance [6–13], due to a negative effect of water in the presence of the hydrophilic alumina carrier [6–14], is pressing the discovery of alternative catalyst formulations including copper as active phase and various oxide carriers and promoters like Al_2O_3 [8,11,14], Cr_2O_3 [15], TiO_2 [14], ZnO [6–13,15,16], ZrO_2 [6–12,17–21], CeO_2 [21] or their combinations [6–12,16–26]. Although ZrO_2 carrier enhances the CO_2-hydrogenation functionality of the Cu–ZnO catalyst, the preparation method controls the activity pattern by affecting texture and dispersion of metal and oxide phases [6–13,20]. Indeed, the reactivity of the Cu–ZnO/ZrO_2 systems depends on neighboring metal and oxide sites driving the activation of H_2 and CO_2 respectively and the consequent formation-hydrogenation of the *formate* intermediate [6,7,9–26].

Therefore, this work is aimed at probing the effects of CeO_2 addition either as promoter or carrier on the structure and CO_2-hydrogenation activity of Cu catalysts in comparison to a reference Cu–ZnO/ZrO_2 catalyst [7,10,11]. The effects of catalyst composition and activation atmosphere on MSA and reactivity of CeO_2-based

* Corresponding author at: Dipartimento di Chimica Industriale ed Ingegneria dei Materiali, Università degli Studi di Messina, Viale F. Stagno D'Alcontres 31, 98166 Messina, Italy. Tel.: +39 090 6765484; fax: +39 090 391518.
E-mail address: Francesco.Arena@unime.it (F. Arena).

0920-5861/$ – see front matter © 2011 Elsevier B.V. All rights reserved.
doi:10.1016/j.cattod.2011.04.038

Table 1
List and physico-chemical properties of the studied catalysts.

Code	Catalyst formulation	Analytical composition							SA ($m^2\ g^{-1}$)	PV ($cm^3\ g^{-1}$)	APD[a] (nm)
		(wt%)				(atomic ratio)					
		CuO	ZnO	ZrO_2	CeO_2	Zn/Cu	Zr/Cu	Ce/Cu			
ZnCuZr	$ZnOCu/ZrO_2$	40	15	43	–	0.4	0.7	0.0	174	0.56	13
CeCuZr	CeO_xCu/ZrO_2	34	–	35	27	0.0	0.7	0.4	117	0.27	9
ZnCuCeZr-1	$ZnOCu/CeZrO_2$	40	13	36	9	0.3	0.6	0.1	162	0.83	20
ZnCuCeZr-2	$ZnOCu/CeZrO_2$	38	13	23	25	0.3	0.4	0.3	107	1.02	39
ZnCuCe	$ZnOCu/CeO_2$	34	11	–	54	0.3	0.0	0.7	61	0.34	22

[a] Average pore diameter (APD, 4 PV/SA_{BET}).

Table 2
TPR data of the calcined catalysts.

Catalyst	Temperature of onset reduction and peak maximum (K)				H_2 consumption	
	$T_{o,red}$	T_{M0}	T_{M1}	T_{M2}	($mmol_{H_2}\ g^{-1}$)	(H_2/Cu)
ZnCuZr	395	–	488	845	5.7	1.13
CeCuZr	383	463	490	–	5.6	1.24
ZnCuCeZr-1	383	473	488	813	6.0	1.25
ZnCuCeZr-2	385	474	493	806	6.0	1.25
ZnCuCe	383	466	495	715	5.6	1.30

Table 3
N_2O chemisorption data of the catalysts reduced under pure and diluted hydrogen.

Catalyst	Activation in pure hydrogen		Activation in diluted hydrogen	
	MSA ($m_{Cu}^2\ g_{cat}^{-1}$)	D_{Cu} (%)	MSA ($m_{Cu}^2\ g_{cat}^{-1}$)	D_{Cu} (%)
ZnCuZr	61	29.1	13	6.0
CeCuZr	18	10.0	6	3.6
ZnCuCeZr-1	50	24.1	25	12.1
ZnCuCeZr-2	38	19.4	45	23.0
ZnCuCe	11	5.9	5	3.0

systems is discussed in the light of the *dual-site* nature of the main reaction path.

2. Experimental

Various Cu-$MeO_x/Zr_aCe_bO_2$ catalysts with a Me/Cu atomic ratio (R) of 0.30–0.35 were prepared via the *reverse co-precipitation under ultrasound field* using the metal nitrate salts as precursors [3–5]. After precipitation, the catalysts were washed, dried at 373 K (16 h) and further calcined in air at 623 K (4 h). The list of catalysts with the relative composition and main physical properties is given in Table 1.

Surface area (SA) and pore volume (PV) were obtained from BET and BJH elaboration of N_2 adsorption/desorption isotherms (77 K) respectively, obtained using a ASAP 2010 (*Micromeritics Instrument*) gas adsorption device [7,10,11].

X-ray diffraction (XRD) analysis in the 2θ range 10–70° was performed using a *Philips XPert* diffractometer operating with Ni β-filtered Cu-Kα radiation at 40 kV and 30 mA and a scan step of 0.05° min^{-1}. The diffraction peaks were identified according to the JCPDS database of reference compounds [27].

Temperature programmed reduction (TPR) measurements in the range of 273–1073 K were performed using a quartz reactor (d_{int}, 4 mm) loaded with 15 mg of catalyst, fed with a 5% H_2/Ar mixture flowing at 60 *stp* mL min^{-1} and heated at the rate of 20 K min^{-1} [7,10,11].

Metal surface area (MSA) and copper dispersion (D_{Cu}) were obtained by the "single-pulse" N_2O titration technique using N_2 as carrier gas and a loop of 0.5 mL [7,10–12]. Before the measurements, the samples were reduced at 573 K (1 h) either in pure or diluted hydrogen (5% H_2/Ar), flushed at 583 K in the N_2 carrier flow (15 min) and then cooled down to 363 K. Dispersion and metal surface area were calculated assuming a $Cu/N_2O = 2$ titration stoichiometry and a surface atomic density of 1.46×10^{19} Cu_{at}/m^2 respectively [7].

Catalyst testing in the hydrogenation of CO_2 was carried out using an Inconel reactor (d_{int}, 6 mm) containing 0.5 g of catalyst (40–70 mesh) diluted with 0.5 g of same-sized SiC in the T range of 453–513 K and at a pressure of 3.0 MPa. The $CO_2/H_2/N_2$ reaction mixture in the molar ratio equal to 3/9/1 was fed at the rate of 80 *stp* mL min^{-1} (GHSV, 8.8 *N* L g_{cat}^{-1} h^{-1}). Prior to each test, the catalyst was reduced *in situ* at 573 K for 1 h either in pure or diluted (5% H_2/Ar) hydrogen flows at atmospheric pressure. The reaction stream was analyzed by a GC equipped with a two-column separation system connected to FID (CH_3OH, CH_3OCH_3) and TCD (CO, N_2, CO_2, H_2), respectively.

3. Results and discussion

3.1. Structural and textural properties

Irrespective of composition the data in Table 1 signal a general negative impact of ceria on surface exposure of both Cu/ZrO_2 and Cu–ZnO systems. Indeed, the reference ZnCuZr catalyst features the largest SA exposure and the progressive replacement of zirconia carrier with ceria results in a straight-line decrease with the Ce molar fraction from 174 to 61 m^2/g (ZnCuCe). Although larger pore volumes (0.83–1.02 cm^3/g) and APD values (20–39 nm) indicate an enhanced accessibility of the ZnCuZrCe-1 and ZnCuZrCe-2 catalysts including both ZrO_2 and CeO_2 in carrier composition (Fig. 1), these data denote a lower efficiency of ceria to promote the textural properties of the Cu–ZnO system in comparison to zirconia [21]. This depends on a poor thermal and chemical stability of ceria and the strong ZrO_2–CeO_2 interaction [28] likely lessening the positive structural effects of zirconia [6–13,20]. Matching the above

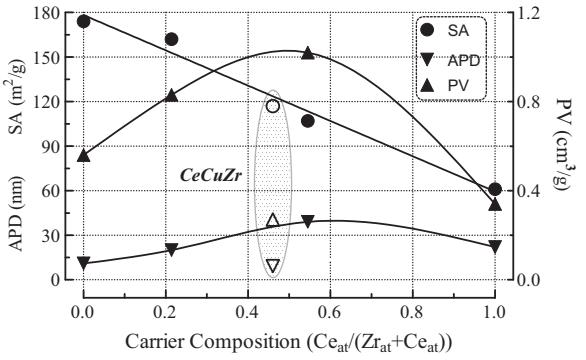

Fig. 1. Influence of the cerium molar fraction on the surface area (SA) of the calcined catalysts.

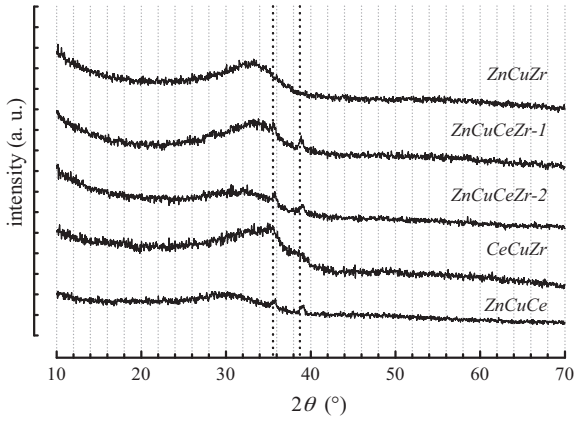

Fig. 2. XRD pattern of the calcined catalysts.

relationship (Fig. 1), the SA of the CeCuZr sample (117 m^2/g) supports this hypothesis also confirming a minor influence of the ZnO promoter on catalyst texture [6–12]. Then, despite the featureless XRD patterns of the calcined samples (Fig. 2) substantiate a high reciprocal dispersion of the oxide phases hindering an appreciable "long-range" crystalline order [7,10,11], tiny signals at 35.6° and 38.7° in all ceria-containing catalysts monitor an incipient crystallization of monoclinic C2/c CuO (*tenorite*) [JCPDS card no. 5.661], confirming that the substitution of ZrO_2 with CeO_2 hinders the Cu precursor dispersion.

The TPR profiles in Fig. 3 show some peculiar differences in the reduction pattern of the active phase, though the onset temperature of reduction ($T_{o,red}$, 375–396 K) and the main peak maximum (T_{M1}, 488–496 K) vary slightly with catalyst composition (Table 2). Moreover, an extent of hydrogen consumption larger than one (H_2/Cu, 1.13–1.30) accounts for the partial reduction of ZnO and/or ZrO_2 at $T > 673$ K [3–5,24–26] and/or ceria in concomitance with that of the Cu precursor [21,29]. The reference ZnCuZr sample shows the highest $T_{o,red}$ value (395 K) and a symmetric reduction peak centered at 488 K. The main T_{M1} reduction peak is slightly shifted to higher temperature in all ceria-containing catalysts (Table 2), whereas a shoulder on its leading edge rises with ceria content until a second maximum is evident for the ZnCuCe sample (Fig. 3). Since the low temperature T_{M0} component is attributable to the reduction of Cu ions in a strong interaction with ceria lattice [21,29], while the upward shift of the T_{M1} peak (Table 2) signal a harder reduction of large crystalline CuO particles [7,10,28–32], the asymmetry of the reduction peak can be taken as a measure of the heterogeneity of the particle size distribution of the Cu precursor.

Indeed, N_2O titration data of the catalysts reduced under pure hydrogen (Table 3) show the largest MSA exposure (61 $m_{Cu}{}^2/g_{cat}{}^1$)

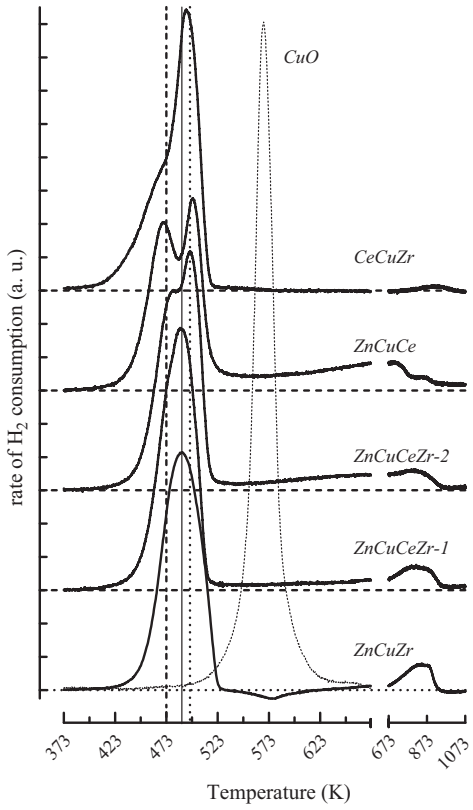

Fig. 3. TPR profiles of the calcined catalysts.

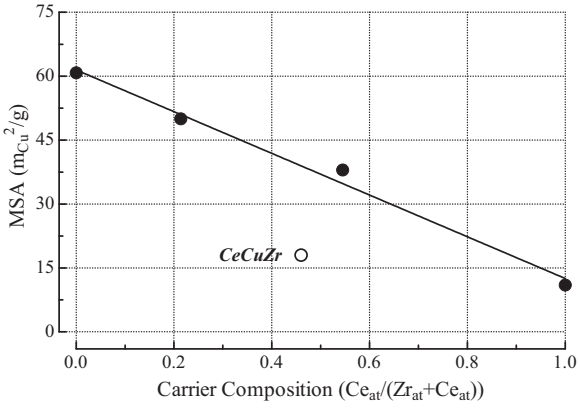

Fig. 4. Influence of the cerium molar fraction on the metal surface area (MSA) of the catalysts activated in pure hydrogen.

for the reference ZnCuZr sample, corresponding to a remarkable *D* value of 29.1% [7,10,11]. This enhanced dispersion of the active phase was previously ascribed to the synergistic effects of ZrO_2 and ZnO promoting the SA exposure and the resistance to sintering of the metal phase respectively [6–11,20]. On the other hand, the straight-line decrease of MSA with the Ce molar fraction (Fig. 4) also signals a negative influence of ceria on Cu dispersion (Table 3), mostly as a consequence of the SA decay (Fig. 1). In fact, these data indicate that the MSA of the Cu–ZnO system is a linear function of the SA of the calcined catalyst (≈35%), while a much lower MSA/SA ratio (≈13%) points out the fundamental influence of ZnO as promoter of the metal dispersion [6,7] accounting for the deviation of the CeCuZr sample from the above correlation (Fig. 4).

With the exception of the ZnCuCeZr-2 sample, the reduction under diluted H_2 leads to a comparatively lower MSA (Table 3)

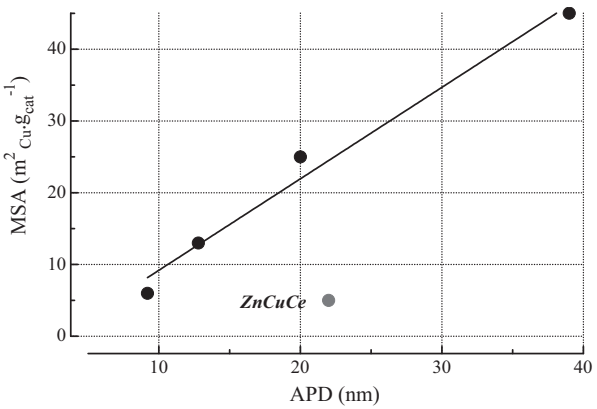

Fig. 5. Influence of the average pore diameter (APD) on the MSA of the catalysts activated in diluted hydrogen (5% H_2/Ar).

that could depend either on sintering or metal surface coverage by oxide promoters [6]. However, a direct relation between MSA and APD signals a positive influence of diluted H_2 on metal surface accessibility of catalysts with larger pore diameters (Fig. 5). Considering the overwhelming partial pressure of the inert component in the case of diluted H_2, this finding can be explained by a negative influence of argon on the counter-diffusion of water produced by the reduction of CuO particles. Just the retention of water inside the pores, due to a much lower diffusion rate of water in argon ($D_{AB} \propto (M_A \cdot M_B)^{-1/2}$), could explain an enhanced sintering of nascent metal clusters. Nevertheless, a complete substitution of ZrO_2 with the reducible CeO_2 carrier enhances the mobility of Cu particles, accounting for the deviation of the ZnCuCe system from the above relationship (Fig. 5).

3.2. Catalytic pattern

The CO_2 hydrogenation activity data in the range of 473–513 K (P, 3.0 MPa), summarized in Table 4 in terms of CO_2 conversion and CH_3OH selectivity values, indicate that the activity pattern depends both on catalyst composition and activation atmosphere. The reference ZnCuZr catalyst reduced in H_2 features a CO_2 conversion raising from 2.1 to 16.4% and a selectivity lowering from 90 to 38% respectively, while the systems missing either ZrO_2 carrier (ZnCuCe) or ZnO promoter (CeCuZr) exhibit considerably worse conversion and selectivity levels (Table 4). On the other hand, an incipient replacement of zirconia with ceria carrier determines a positive effect on the activity pattern of the ZnCuZrCe-1 system mostly in terms of selectivity, whereas a further replacement of zirconia causes a worsening of the catalytic performance in terms of activity (Table 4). Then, the above data can be summarized in the following activity scale referred to the methanol yield (Y, %) in the range of 453–513 K respectively:

$$\text{ZnCuCeZr-1}\,(2.8\text{–}8.4) > \text{ZnCuZr}\,(1.9\text{–}6.2) > \text{ZnCuCeZr-2}\,(1.7\text{–}5.7) > \text{CeCuZr}\,(1.1\text{–}3.7) \approx \text{ZnCuCe}\,(0.6\text{–}4.0)$$

The activation under the diluted hydrogen stream improves the activity of all the catalysts including both ZnO and CeO_2, while the CeCuZr and reference ZnCuZr systems show a lower activity and only slightly higher methanol selectivity (Table 4). In particular, the ZnCuCeZr-1 and ZnCuCeZr-2 samples feature 20–30% higher conversion at any temperature though the selectivity keeps at the same levels of samples activated under pure hydrogen. While, the ZnCuCe sample shows 2–3 times greater conversion values than the sample activated under pure hydrogen despite no remarkable changes in selectivity (Table 4). Then, the ranking of the catalysts relative to the methanol yield (%) is the following:

$$\text{ZnCuCeZr-1}\,(2.9\text{–}8.6) > \text{ZnCuCeZr-2}\,(2.0\text{–}7.4) > \text{ZnCuCe}\,(1.6\text{–}6.3) \approx \text{ZnCuZr}\,(1.7\text{–}5.4) \gg \text{CeCuZr}\,(1.0\text{–}2.9)$$

Although thermodynamic equilibrium data at the various temperatures (Table 4) indicate that the ZnCuZrCe-1 system exhibits the best catalytic behavior both under kinetic ($T \leq 473$ K) and thermodynamic ($T > 473$ K) regime regardless of the reducing atmosphere, the above reactivity scales cannot be related to the metal Cu exposure according to Fig. 6, showing no relation between the changes in MSA and Y_{CH_3OH} of catalysts reduced under pure and diluted hydrogen streams. According to previous findings, this indicates that the MSA is not the key-property governing the CO_2-hydrogenation functionality of promoted Cu systems [6–15,20–22]. In addition, it is evident that the positive effect of the activation in diluted H_2 on the reactivity of the Cu–ZnO system rises with the cerium content of the carrier (Fig. 6). In fact, because of rather different surface exposure (Table 1), a proper comparison of the functionality of the various systems is possible on the basis of the

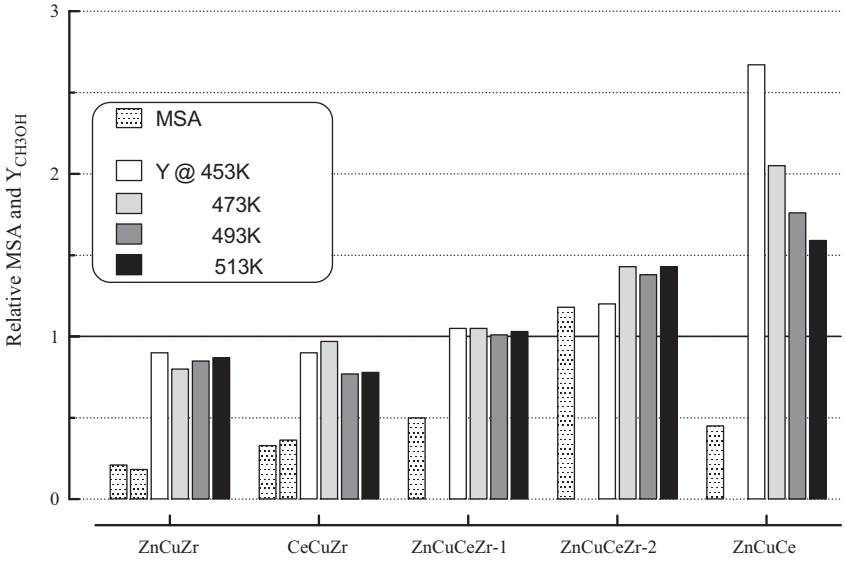

Fig. 6. MSA and Y_{CH_3OH} in the range of 453–513 K of the catalysts activated in diluted hydrogen normalized to that of the catalysts activated in pure hydrogen.

Table 4
CO_2-hydrogenation data of the catalysts activated either under pure or diluted hydrogen and relative equilibrium data in the range of 453–513 K (P_R, 3.0 MPa; GHSV, 8.8 $NL\,g^{-1}\,h^{-1}$).

Catalyst	T_R, 453 K X_{CO_2}–S_{MeOH} (%)			T_R, 473 K X_{CO_2}–S_{MeOH} (%)			T_R, 493 K X_{CO_2}–S_{MeOH} (%)			T_R, 513 K X_{CO_2}–S_{MeOH} (%)		
	Pure H_2	Diluted H_2	Equilibrium	Pure H_2	Diluted H_2	Equilibrium	Pure H_2	Diluted H_2	Equilibrium	Pure H_2	Diluted H_2	Equilibrium
ZnCuZr	2.1–90	1.7–100		4.6–75	3.3–84		9.5–54	6.4–68		16.4–38	11.8–46	
CeCuZr	1.1–100	1.0–99		2.1–71	1.9–76		4.7–58	3.4–62		9.4–39	6.8–42	
ZnCuCeZr-1	2.9–97	3.2–92	30–97	5.7–88	6.4–82	25–91	9.9–74	11.4–65	22–75	14.7–57	16.9–51	21–54
ZnCuCeZr-2	1.7–100	2.2–93		3.6–80	4.8–86		7.1–65	8.6–74		11.3–46	13.3–56	
ZnCuCe	0.6–100	1.6–100		1.8–87	3.6–89		3.5–77	6.0–79		6.4–62	10.7–59	

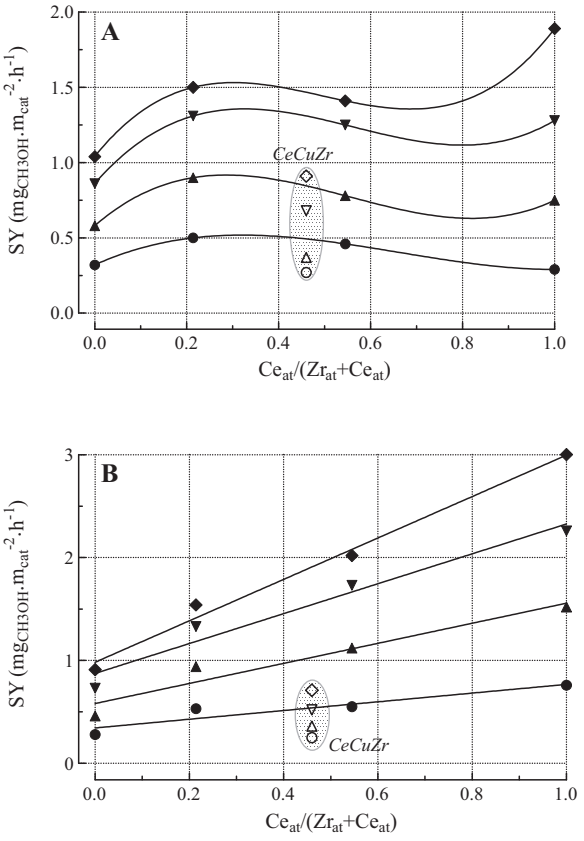

Fig. 7. Influence of the cerium molar fraction on methanol surface yield (SY) in the range of 453–513 K of catalysts activated in pure (A) and diluted hydrogen (B).

surface methanol yield (SY, $mg_{CH_3OH}\,m_{cat}^{-2}\,h^{-1}$), which depends on cerium molar fraction as shown in Fig. 7. Despite the marked lowering in activity recorded for Cu–ZnO catalysts with higher ceria contents (Table 4), the surface methanol yield of the systems reduced in pure hydrogen are comparable regardless of the carrier composition (Fig. 7A). Therefore, the negative influence of ceria depends on the poorer efficiency to promote surface area and catalyst texture in comparison to zirconia [21]. While, systematically lower SY values of the CeCuZr catalyst substantiate the role of ZnO as electronic promoter of the metal Cu phase [6–11]. On the other hand, the reduction in diluted H_2 implies an evident promoting role of ceria on the surface functionality of the Cu–ZnO system in the whole range of temperature, the extent of which is a straight function of the loading (Fig. 7B). While the data relative to the CeCuZr sample still confirm the crucial role of ZnO to enhance the catalytic activity of Cu (Fig. 7), the lack of relationship between activity and MSA, also with reference to the influence of the activation atmosphere (Fig. 6), can be explained by the contribution of some oxide sites at metal/oxide interface to the main reaction path [6–12,20–26]. In this context, the peculiar solid-state reactivity of ceria [21,28,29] enhancing the interaction between metal and promoters could account for the improved surface functionality of the Cu–ZnO system [32]. In fact, an intimate contact of metal and oxide phases enhances the density of CO_2 adsorption-activation sites at the Cu/oxide(s) interface, perhaps in the form of Cu–Ce^{3+} [32], reflecting thus in higher concentration of the *formate* intermediate and, definitely, in higher reaction rates [6–12,20,21,32]. Further, a larger adsorption and an easy spillover of active hydrogen species across ceria lattice [21,28] can well contribute to speed up the hydrogenation rate of the formate intermediate [21,22]. This effect is particularly evident for the reduction in diluted hydrogen since a shallow reduction of ceria likely prevents an extensive

phases segregation hindering the above effects on catalysts activated in pure hydrogen [6,21,28].

4. Conclusions

The effects of ceria promoter and activation atmosphere on the CO_2-hydrogenation functionality of Cu catalysts have been addressed.

Ceria carrier promotes the surface functionality of the Cu–ZnO system though a negative influence on catalyst texture and metal surface area in comparison to ZrO_2.

ZnO plays a fundamental role as promoter of both dispersion and catalytic functionality of the metal copper phase.

The activation in diluted hydrogen enhances the surface functionality of ceria-promoted Cu–ZnO catalysts.

The lack of relationship between MSA and catalytic activity substantiates the *dual-site* nature of the main reaction path, confirming the fundamental role the metal/oxide(s) *interface* on the CO_2-hydrogenation functionality of Cu-based catalysts.

References

[1] N. Tsubaki, M. Ito, K. Fujimoto, J. Catal. 197 (2001) 224.
[2] G.A. Olah, A. Goeppert, G.K.S. Prakash, Beyond Oil and Gas: The Methanol Economy, Wiley-VCH Verlag GmbH & Co. KGaA, Weinheim, 2006.
[3] Energy Information Administration (EIA), Washington DC, February 2003.
[4] J.B. Hansen, B. Voss, F. Joensen, I. Sigurdardottir, SAE Paper n° 950063 (1995).
[5] T. Fleisch, A. Basu, M.J. Gradassi, J.G. Masin, Stud. Surf. Sci. Catal. 107 (1997) 117.
[6] X.-M. Liu, G.Q. Lu, Z.-F. Yan, J. Beltramini, Ind. Eng. Chem. Res. 42 (2003) 6518.
[7] F. Arena, K. Barbera, G. Italiano, L. Spadaro, F. Frusteri, J. Catal. 249 (2007) 183.
[8] Y. Zhang, J. Fei, Y. Yu, X. Zheng, Energy Convers. Manage. 47 (2006) 3360.
[9] C. Yang, Z. Ma, N. Zhao, W. Wei, T. Hu, Y. Sun, Catal. Today 115 (2006) 222.
[10] F. Arena, G. Italiano, K. Barbera, G. Bonura, L. Spadaro, F. Frusteri, Appl. Catal. A 350 (2008) 16.
[11] F. Arena, G. Italiano, K. Barbera, G. Bonura, L. Spadaro, F. Frusteri, Catal. Today 143 (2009) 80.
[12] F. Arena, L. Spadaro, O. Di Blasi, G. Bonura, F. Frusteri, Stud. Surf. Sci. Catal. 147 (2004) 385.
[13] T. Inui, H. Hara, T. Takeguchi, J.-B. Kim, Catal. Today 36 (1997) 25.
[14] K.K. Bando, K. Sayama, H. Kusama, K. Okabe, H. Arakawa, Appl. Catal. A 165 (1997) 391.
[15] S.-H. Kang, J.W. Bae, H.-S. Kim, G.M. Dhar, K.-W. Jun, Energy Fuels 24 (2010) 804.
[16] L. Ma, T. Tran, M.S. Wainwright, Top. Catal. 22 (2003) 295.
[17] M. Saito, T. Fujitani, M. Takeuchi, T. Watanabe, Appl. Catal. A 138 (1996) 311.
[18] K.-D. Jung, A.T. Bell, J. Catal. 193 (2000) 207.
[19] J. Liu, J. Shi, D. He, Q. Zhang, X. Wu, Y. Liang, Q. Zhu, Appl. Catal. A 218 (2001) 113.
[20] X. Guo, D. Mao, G. Lu, S. Wang, G. Wu, J. Catal. 271 (2010) 178.
[21] K.A. Pokrovski, A.T. Bell, J. Catal. 241 (2006) 276.
[22] I.A. Fisher, A.T. Bell, J. Catal. 172 (1997) 222.
[23] T. Kakumoto, T. Watanabe, Catal. Today 36 (1997) 39.
[24] K.-W. Jun, W.-J. Shen, K.S. Rama Rao, K.-W. Lee, Appl. Catal. A 174 (1998) 231.
[25] J. Sloczynski, R. Grabowski, A. Kozlowska, P. Olszewski, J. Stoch, J. Skrzypek, M. Lachowska, Appl. Catal. A 278 (2004) 11.
[26] Y. Ma, Q. Sun, D. Wu, W.-H. Fan, Y.-L. Zhang, J.-F. Deng, Appl. Catal. A 171 (1998) 45.
[27] ASTM Powder Diffraction Files, Joint Committee on Powder Diffraction Standards, Park Lane, PA, 1979.
[28] A. Trovarelli, Catal. Rev. Sci. Eng. 38 (1996) 439.
[29] F. Arena, R. Giovenco, T. Torre, A. Venuto, A. Parmaliana, Appl. Catal. B 45 (2003) 51.
[30] S. Bennici, A. Auroux, C. Guimon, A. Gervasini, Chem. Mater. 18 (2006) 3641.
[31] W.-P. Dow, Y.-P. Wang, T.-J. Huang, J. Catal. 160 (1996) 155.
[32] J.B. Wang, H.-K. Lee, T.-J. Huang, Catal. Lett. 83 (2002) 79.